Nanoscale

PAPER

View Article Online
View Journal | View Issue

Cite this: *Nanoscale*, 2019, **11**, 17293

Two-photon based pulse autocorrelation with CdSe nanoplatelets†

Michael T. Quick,‡[a] Nina Owschimikow,[a] Ali Hossain Khan,[b,c] Anatolii Polovitsyn,[b,c] Iwan Moreels,[b,c] Ulrike Woggon[a] and Alexander W. Achtstein‡[a]

Received 19th July 2019,
Accepted 6th September 2019

DOI: 10.1039/c9nr06156h

rsc.li/nanoscale

We investigate broadband two-photon absorption autocorrelators based on II–VI semiconductor nanoplatelets as an alternative to common second harmonic generation based techniques. As compared to bulk materials the exceptionally high enhancement of two-photon absorption in these 2D structures results in very efficient two-photon absorption based autocorrelation detected *via* PL emission. We compare the results with TPA autocorrelation in CdS bulk as well as SHG based autocorrelation in β-barium borate. We show that CdSe nanoplatelet based autocorrelation can exceed the efficiency of conventional methods by two orders in magnitude, especially for short interaction length, and allows a precise pulse-width determination. We demonstrate that very high two-photon absorption cross sections of the nanoplatelets are the basis for this effective TPA autocorrelation. Based on our results with II–VI nanoplatelets efficient broadband autocorrelation with more than ~100 nm bandwidth and very high sensitivity seems feasible.

1. Introduction

Two-photon absorption (TPA) in semiconductor nano materials receives growing interest in photonics, imaging and medical research. Extensive studies have been performed with regard to the size, shape, *k*-vector and spectral dependence of two-photon absorption in quantum dots, -rods and nanoplatelets.[1–11] Applications span from two-photon lithography,[12] optical amplification and lasing,[13–15] possible upconversion in solar cells[16] to two-photon microscopy *in vivo*,[17] bioimaging and -detection[18,19] to cancer therapy.[20] Numerous concepts contain semiconductor nanoparticles or have suggested their further use in nonlinear applications. The research focus relates to their promising nonlinear properties, like for instance their very high TPA coefficients $\sigma^{(2)}$ or their bandgap and spectral tunability *via* nanostructure size.[17,21–23] Recently it has been demonstrated that anisotropic confined systems, like II–VI semiconductor nanoplatelets,[23–29] with strong *z*-confinement but weak lateral confinement exhibit due to their large coherence volumina and their small exciton Bohr radii (high exciton binding energies) extremely high two-photon absorption cross sections of up to 10^8 GM.[5] They scale quadratically with the area of the 2D structures.[21] These structures offer unprecedented nonlinearities (both per particle or per unit volume) with respect to the two-photon absorption coefficient β (reaching ~100 times the bulk value). Hence we investigate in this letter temporal cross- and autocorrelation of laser pulses *via* two-photon absorption as an application of these high nonlinearities.

In the early 90s TPA based autocorrelation using bulk materials has been proposed as a replacement of the hitherto established nonlinear processes.[30,31] In this context not the two-photon absorption itself or the TPA based re-emission fluorescence have been used, but the TPA induced e–h pairs creating a photocurrent, often measured directly in a photodiode, whose active region already acts as a two-photon absorber.[32–38] This idea has been extended to commercial diodes operated as unbiased photodiodes.[39,40] However, the sensitivity of these devices is limited by the rather small nonlinearities of the quasi bulk semiconductor materials used *e.g.* in the intrinsic layer of a PIN diode and the very limited absorption probability within typical intrinsic layer thicknesses.

Nonlinear semiconductor nano materials offer several advantages as compared to bulk transparent nonlinear optical crystals. In contrast to SHG performed *e.g.* in β-barium borate (BBO), TPA does not require phase matching between the fundamental waves and the SHG, as the detected signal is formed after two-photon absorption by spontaneously re-emitted photons with the semiconductor bandgap energy. Especially

[a]*Institute of Optics and Atomic Physics, Technical University of Berlin, Strasse des 17. Juni 135, 10623 Berlin, Germany. E-mail: alexander.achtstein@tu-berlin.de*
[b]*Instituto Italiano di Tecnologia, via morego 30, 16163 Genova, Italy*
[c]*Department of Chemistry, Ghent University, krijgslaan 281-S3, 9000 Gent, Belgium*

†Electronic supplementary information (ESI) available. See DOI: 10.1039/C9NR06156H

‡These authors contributed equally to this work.

regarding conversion efficiency and sensitivity TPA can outpace SHG techniques by orders of magnitude.[21,36,40] Most interesting, however, is the possibility of very large autocorrelation bandwidth. For broadband SHG autocorrelation in *e.g.* BBO, LBO, or similar materials, dispersion requires to use increasingly thin crystals for broadband pulses. As the conversion efficiency increases quadratically with the product of crystal length and $\chi^{(2)}$,[41] (under the assumption of no pump depletion) short crystals have low efficiency so that materials with high nonlinearities are desired. TPA based autocorrelation with nanocrystals does not experience this problem as explained above. The need for highly stable ultra-broadband autocorrelation is further justified by the growing field of fs and attosecond physics, where fs and sub femtosecond pulse lengths[42] demand *e.g.* ~100 nm or even octave spanning autocorrelators.

Many commercial and non-commercial autocorrelation devices based on different principles are currently on the market, however, the usage of nano materials for TPA autocorrelation is less investigated.[40] Moreover, apart from choosing usual co-propagating beam Michelson interferometer type setups, also non-collinear geometries allow to cross correlate two light pulses of different frequency, *e.g.* by TPA, satisfying the condition $h\nu_1 + h\nu_2 \geq E_g$.[21] Hence we demonstrate in the following as a proof of concept efficient TPA autocorrelation with 2D CdSe nanoplatelets (NPLs), detected *via* PL, using their exceptionally high TPA nonlinearity. In this paper we will at first target the autocorrelation and then discuss its high efficiency based on the determination of the TPA cross section of CdSe nanoplatelets.

2. Results and discussion

2.1. Pulse width

Two CdSe nanoplatelet samples of different lateral platelet sizes are tested here with regard to their ability to autocorrelate 171 fs duration of 800 nm reference laserpulses efficiently. The schematic measurement setup is depicted in Fig. 1. For a detailed description of the measuring configuration and process we refer to the Methods section. In order to assess the functionality, we compare the results to the autocorrelation obtained *via* common SHG in a β-BaB_2O_4 crystal (BBO) and additionally to the autocorrelation by two-photon absorption in a CdS bulk sample. CdSe nanoplatelets of 24 × 12 nm^2 (288 nm^2) and 29 × 6 nm^2 (174 nm^2) area and 4.5 monolayers (ML) thickness dispersed in polystyrene (PS) were used. As opposed to the SHG in BBO, the spontaneous emission (at semicondutor bandgap) upon two-photon absorption is used to autocorrelate the laser pulses in CdS and CdSe. The acquired SHG and PL signal spectra in the temporal overlap of both methods are displayed in Fig. 2. We see that it is feasible to measure pulse autocorrelation with CdSe nanoplatelets. As an autocorrelation measurement does not yield the actual pulse width directly, we need to take the fixed ratio of the FWHM of the autocorrelation and pulse width into account.

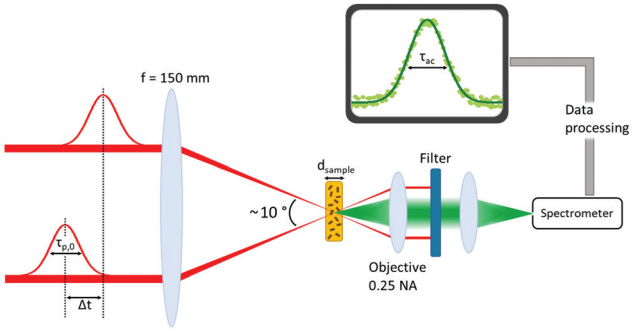

Fig. 1 Measurement setup for acquisition of TPA (SHG) autocorrelation curves using a two beam scheme with relative delay. In case of SHG a BBO is used of the two photon absorber (CdSe platelets or CdS crystal). In the BBO case the objective is removed, since a collimated SHG beam is generated.

By definition the second order correlation function $G^{(2)}(t)$ in time is given by a temporal convolution of two pulse intensities $I_A(t)$ and $I_B(t)$.

$$G^{(2)}(\tau) = \int_{-\infty}^{\infty} I_A(t) I_B(t+\tau) \mathrm{d}t \quad (1)$$

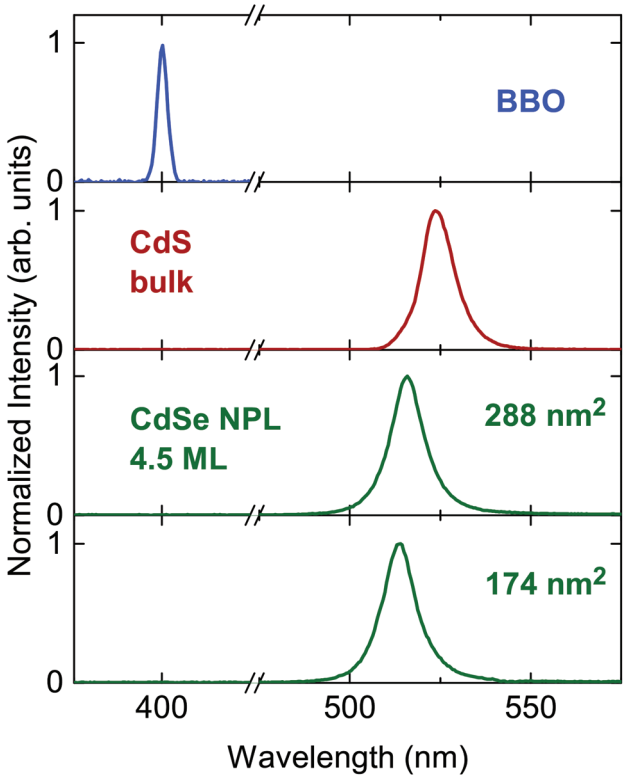

Fig. 2 Normalized spectra resulting from second harmonic generation (blue), photoluminescence (PL) of CdS bulk (red) and PL of CdSe NPLs (green). In case of the semiconductor samples the emission is red-shifted with respect to SHG since the re-emission occurs at the bandgap wavelength. Spectra correspond to maximal temporal overlap of two 800 nm pulses within each sample.

Fourier transformation ($\mathscr{F}$) allows to express this convolution also as a product in frequency domain. For Gaussian temporal pulses it can be shown that the FWHM τ_p of the pulse, is related to its autocorrelation width τ_{ac} *via* $\tau_p = \tau_{ac}/\sqrt{2}$.[43] Fig. 3 shows the four resulting autocorrelation curves of our samples, which are listed in Table 1. We use a BBO crystal as an autocorrelation reference and define the relative deviation of the FWHM as $\Delta = |(\tau - \tau_{BBO})/\tau_{BBO}|$, an indicator for the agreement among the different studied autocorrelation techniques. The deviation for the CdSe platelets is below 4%, thus giving excellent agreement with the BBO reference, while for the CdS bulk sample it is 9%, expectedly bigger due to considerable pulse broadening in CdS. Pulse broadening within the NPL samples due to dispersion can be shown to have no relevant effect in the two samples.[44] This is the case because group velocity dispersion around 800 nm is low in polystyrene, the embedding matrix of the dispersed NPLs.[45] The pulse broadening of an incoming pulse is given by:

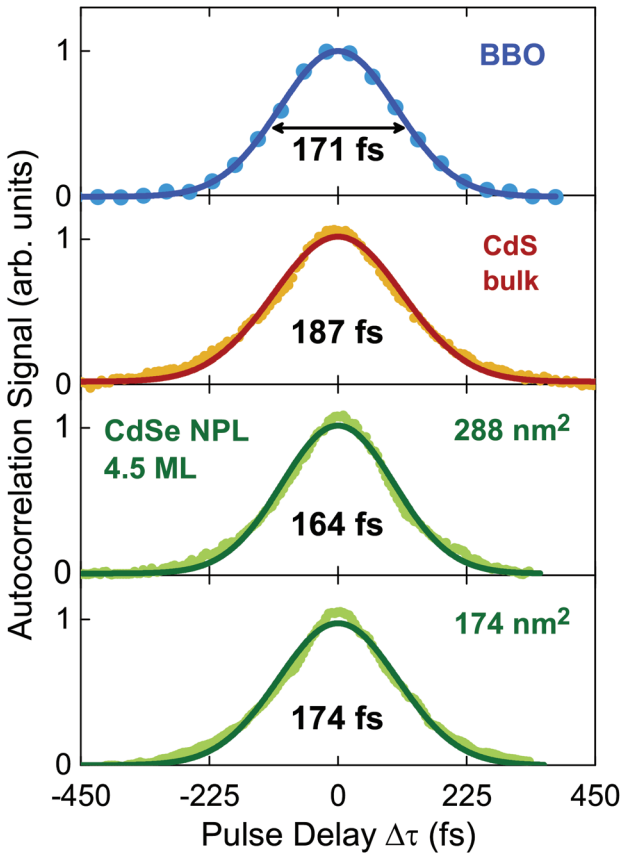

Fig. 3 Normalized autocorrelation curves resulting from different methods and samples, respectively *vs.* relative pulse delay in fs. Data were fitted assuming a Gaussian pulse shape, characteristic for the Coherent Mira 900 HP fs laser, as clearly seen for the BBO data. Autocorrelations are performed *via* SHG in BBO (blue), TPA in CdS bulk (red) and TPA in two different CdSe NPL samples (green) of distinct size *via* delaying one 800 nm beam *vs.* the other. The autocorrelation's FWHM is connected to the pulse FWHM τ_p by $\tau_p = \tau_{ac}/\sqrt{2}$.[43] The measured pulse width τ_p are indicated.

Table 1 Experimentally determined $\tau_{p,1}$ and corresponding estimated pulse durations (eqn (2)) of 171 fs pulses passing samples of length $\bar{z}$ (eqn (2)) as well as parameter C

	CdSe NPL			
	174 nm²	288 nm²	CdS	BBO
$\tau_{p,1}$ (fs) meas.	174	164	187	171
$\tau_{p,1}$ (fs) est.	174	174	191	171
d_{sample} (mm)	0.95	0.90	0.50	0.50
$\bar{z}$ (mm)	0.49	0.57	0.50	—
C (cm⁴ GW⁻²)	41	76	4.2×10^3	—

$$\tau_{p,1} = \tau_{p,0}\left[\left(1 + aB\left(\frac{\partial^2 n}{\partial \lambda^2}\right)\frac{\bar{z}}{{\tau_{p,0}}^2}\right)^2 + \left(B\left(\frac{\partial^2 n}{\partial \lambda^2}\right)\frac{\bar{z}}{{\tau_{p,0}}^2}\right)^2\right]^{\frac{1}{2}} \quad (2)$$

Here, τ_0 and τ_1 give the Gaussian pulse FWHM before and after passing the sample, $\bar{z}$ is an effective emission depth within the sample and a is the (linear) chirp parameter. a is related to the instantaneous frequency $\omega(t)$ by $\omega(t) = \omega_c + d\Phi/dt = \omega_c + 2at/{\tau_{p,0}}^2$ within our Gaussian pulse of central frequency ω_c. B is a proportionality constant, given by $B = ({\lambda_0}^3 2\ln(2))/(\pi {c_0}^2)$. The chirp parameter a relates to a spectral phase of a Gaussian pulse (chirp) and alters its time-bandwidth product.[46] The pulse impinging on the sample is linearly chirped, as common for Ti:Sa laser systems, which are not bandwidth limited. a can be estimated from the time-bandwidth product of the laser source *via* $\Delta\omega \times \tau_p = 4\ln(2)\sqrt{1+a^2}$ (with $a = 1.7$ for our laser system). Second, to calculate the effective emission depth $\bar{z}$, reabsorption during propagation of two-photon induced PL emission through the samples has to be considered. The effective emission depth due to reabsorption is calculated by:

$$\bar{z} = \frac{\int_0^L dz\, z\left(\frac{\partial I_F}{\partial z}\right)e^{-(L-z)\alpha}}{\int_0^L dz\left(\frac{\partial I_F}{\partial z}\right)e^{-(L-z)\alpha}} = L - \frac{1}{\alpha} + \frac{L}{e^{L\alpha}-1} \quad (3)$$

L gives the sample's thickness, I_F the emission intensity and α represents the linear absorption coefficient. The relation above holds, as the Rayleigh length (2.5 mm) of the used 15 cm focussing lens for excitation is greater than the sample thickness (0.5 mm). The TPA induced luminescence emission per unit length ($\partial I_F/\partial z$) and the incoming excitation wave's intensity I_{exc} (800 nm) are connected for TPA *via*:

$$\left(\frac{\partial I_F}{\partial z}\right) = -\frac{1}{2}\left(\frac{\partial I_{exc}}{\partial z}\right)\eta, \quad (4)$$

where η is the emission quantum yield. In the case of bulk CdS reabsorption occurs, which is not relevant in the dilute nanoplatelet doped polymers, so that only photons created near the very end of the sample are detected while for the platelet doped samples the emission originates on average from near the center (see Table 1). The impinging Gaussian beam diameter alters negligibly while passing through the samples, since the sample is much thinner than the Rayleigh length, so that the derivative in brackets is constant. Table 1

shows the pulse width measurement results for our samples, all of which are in very good agreement with the BBO reference. The deviation of the predicted pulse durations relative to BBO is low (<4%) for the NPLs and highest (~12%) for the CdS bulk sample, while the latter is mainly due to pulse broadening in CdS, as seen in Table 1 from the broadening estimates $\tau_{p,1est.}$. For both of our NPLs, variation of the input power, and hence the intensity has no significant influence on the measured pulse durations (see ESI† for details). However, for a nonlinear measurement this is still a very good (deviation) value for the nanoplatelets. Hence we have shown that CdSe nanoplatelets allow accurate and efficient TPA based autocorrelation. In the following we assess the impact of the high two-photon absorption nonlinearity in CdSe nanoplatelets for autocorrelation.

2.2. Power series and TPA cross section

Fig. 4 displays the excitation intensity dependent emission of the NPLs and CdS bulk. The observed linear behavior in the logarithmic presentation corresponds to a near quadratic intensity dependence. Beam A and B were switched on independently to acquire the two data sets. The unequal excitation intensities of Beam A and B, respectively, arise due to slight differences in the beam profiles at the same position. Influences from TPA saturation can be excluded, since in case of II–VI semiconductor nanocrystals a saturation intensity in the order of 200 GW cm^{-2} is expected,[2] which translates to an average power of at least 60 W needed in our measurements, orders of magnitude higher as compared to our measurement range. Equally it has been shown, that for CdS bulk no saturation effects are observed below an excitation intensity of 6 GW cm^{-2}.[2,5]

To understand why CdSe NPLs are suitable for efficient second order autocorrelation, we target their TPA nonlinearity quantitatively in the next section. We use our intensity dependent measurements for TPA cross section calculation, which will demonstrate their considerably higher nonlinearity as compared to bulk. The acquired signal can be understood as the total emission intensity $I_{F,out}$ modified by an excitation and detection efficiency φ (a setup constant for each beam). Likewise, the signal S is proportional to the square of the incoming excitation wave's intensity I_{exc}.

$$S(I_{exc}) = \varphi I_{F,out} = C{I_{exc}}^2 \tag{5}$$

The conversion figure of merit C is directly obtained from fitting the data (Fig. 4) and used to retrieve the TPA cross section. The total number of PL photons leaving the sample, and hence the intensity $I_{F,out}$, is diminished by reflection R (of the excitation) at the sample's front surface when entering and reflection of the emitted PL photons when exiting the sample.

$$\begin{aligned} I_{F,out} &= (1-R_{in})^2(1-R_{out})\int_0^L dz\left(\frac{\partial I_F}{\partial z}\right) \\ &= (1-R_{in})^2(1-R_{out})\left(\frac{\partial I_F}{\partial z}\right)L \end{aligned} \tag{6}$$

$R = (n(\lambda) - 1)^2/(n(\lambda) + 1)^2$ stands for the intensity reflection coefficient for entering or leaving the sample. They depend on the excitation and emission wavelength. Again, the derivative is linked to the attenuated excitation wave by the former introduced eqn (4). As the sample is transparent for the laser at 800 nm, no linear absorption is taken into account and the derivative of I_{exc} can be solely related to the TPA coefficient β by $(\partial I_{exc}/\partial z) = -\beta {I_{exc}}^2$. Using the eqn (4) and eqn (6) yields:

$$I_{F,out} = \frac{1}{2}L\beta\eta(1-R_{in})^2(1-R_{out}){I_{exc}}^2 = \frac{S(I_{exc})}{\phi} = \frac{C{I_{exc}}^2}{\phi}. \tag{7}$$

Considering ϕ a system constant, it is possible to find β for a sample under test (s), once a reference (r) is known.

$$\frac{C_r}{C_s} = \frac{\beta_r\eta_r L_r(1-R_{r,in})^2(1-R_{r,out})}{\beta_s\eta_s L_s(1-R_{s,in})^2(1-R_{s,out})} \tag{8}$$

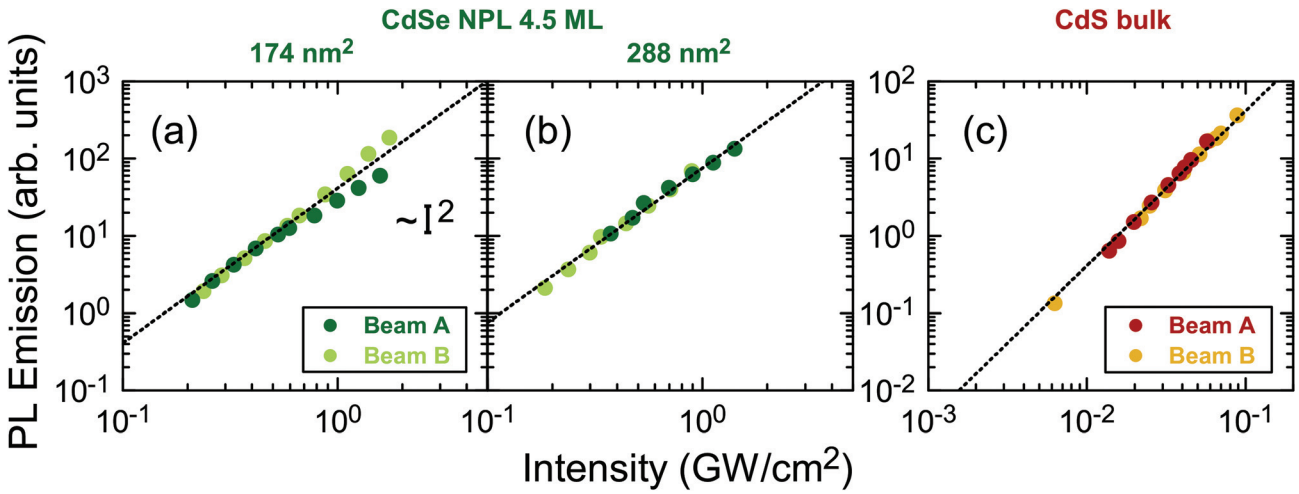

Fig. 4 PL signal *vs.* the beam temporal and spatial peak intensity in GW cm^{-2} for NPLs of two different areas 174 nm^2 (a) and 288 nm^2 (b) as well as for CdS bulk (c). The quadratic fit according to eqn (5) (shown as a dotted fit line on the logarithmic scale) yields a factor C, the conversion figure of merit.

To apply eqn (8) for nanocrystalline materials, a relation between β and the particle TPA cross section $\sigma^{(2)}$ has to be used:

$$\beta_{s,\,\mathrm{eff}} = \frac{\sigma^{(2)} f_V}{h\nu V_{p,s}}, \tag{9}$$

with $V_{p,s}$ the semiconductor nanoparticle volume and f_V its volume fraction in the sample.[47] In case of NPLs dispersed in a matrix, an effective TPA coefficient $\beta_{s,\mathrm{eff}}$ is used. This takes into consideration, that the (nonlinear) material property $\beta_{s,\mathrm{Mat}}$ (of a virtual, bulk like material) is altered through the finite, less than 100%, volume filling of the in the matrix embedded nonlinear particles. This results in an effective $\beta_{s,\mathrm{eff}}$ for the NPL doped polymer sample. f_V can be determined *via* measuring the sample absorbance, once the nano particle (linear) intrinsic absorption coefficient μ_i is known.[48] We obtain $f_V = 6.7 \times 10^{-5}$ for the 288 nm^2 and $f_V = 7.1 \times 10^{-5}$ for the 174 nm^2 NPLs (see ESI†).

$$\sigma^{(2)} = \frac{C_s h\nu V_{p,s} L_r \beta_r \eta_r}{C_r f_V L_s \eta_s} \frac{(1-R_{r,in})^2 (1-R_{r,out})}{(1-R_{s,in})^2 (1-R_{s,out})} \tag{10}$$

Taking CdS bulk as a reference (β_r = 8.8 cm GW^{-1} (ref. 2)) and using eqn (10) with the results given in this work, TPA cross sections of 3.8×10^6 GM (24 × 12 nm^2 CdSe NPL) and 7.7×10^5 GM (29 × 6 nm^2 CdSe NPL) are obtained, considering the quantum yields η of the CdSe samples (both 15%) and reference (6.2%). We refer to ESI† for a detailed calculation. These results are in good agreement with the very high TPA cross sections obtained in *z*-scan and two-photon PLE in ref. 5 for platelets of comparable size. Hence the outcome substantiates that CdSe nanoplatelets with their extremely high nonlinearities are ideal to build high efficiency and low intensity pulse characterization autocorrelators. This will be addressed in the following.

For SHG to occur, *e.g.* in a BBO crystal, coherent interaction between the incoming photons is required as well as phase matching between the fundamental and generated second harmonic field. This requires critical angle or thermal phase matching (*e.g.* in birefringent media), periodically poled (pp)-crystals or very thin crystals, where walk off and phase lag are not limiting the performance. However, for broadband autocorrelation the crystals need to be thin due to group velocity dispersion and mismatch limiting the bandwidth. Hence materials with high nonlinearities are desired, as suggested in the introduction. Here TPA materials with high cross sections come into play, as they do not require phase matching of the fundamental and converted photons, since re-emission after two-photon excitation is spontaneous and incoherent so that there can be no back conversion of the generated radiation into the fundamental beam. As an example for the high efficiency we compare the efficiency of a very thin, dense 10 μm layer of nanoplatelets with 3.7×10^6 GM (and assumed fill factor 100%) with a BBO of identical thickness at 10 GW cm^{-2} at 800 nm, typical power densities for a ~100 MHz repetition rate, ~100 fs Ti:Sa laser system, using ~13 mW focused by a 0.2 NA objective. Due to the extremely thin crystal assumption the conversion efficiency is only ~5×10^{-2} % for the BBO, calculated using ref. 49 and taking into account that the Rayleigh length of the beam (>10 micron) is not smaller than the sample thickness. Estimating the TPA efficiency[21] by $\varphi = 1 - 1/(1 + \beta_{\mathrm{Mat}} L I_{\mathrm{exc}})$ up to 80% is feasible, given the parameters above. For the intrinsic TPA coefficient β_{Mat} of the NPLs itself, which allows comparison to bulk materials, we calculate β_{Mat} = 392 cm GW^{-1} for the larger 24 × 12 nm^2 NPL and β_{Mat} = 122 cm GW^{-1} for the 29 × 6 nm^2 NPL *via* $\beta_{\mathrm{Mat}} = \beta_{\mathrm{eff}}/f_V$ from the obtained cross sections above *via* eqn (9). Furthermore, using a luminescence quantum yield η of 15% for NPLs, the conversion total efficiency $\tilde{\varphi}$ yields $\tilde{\varphi} = \varphi \times \eta$ = 12 %.

For our setup we were able to record autocorrelation traces down to <1 mW beam power. The sensitivity may be extended using a shorter focal length focusing lens, resulting in higher excitation power in the sample. However we did not use shorter lenses, to maintain our setup in a condition, where the sample length is smaller than the Rayleigh length of the lens, to be able to do quantitative referencing of TPA cross sections. The measurable range of input power is limited to below 200 GW cm^{-2} (60 W CW equivalent), the above mentioned TPA saturation intensity.

Contrasting the calculations for CdSe nanoplatelets and BBO we find, that the conversion efficiencies of such NPLs can exceed equivalent SHG in BBO by two orders of magnitude. In a similar manner, the efficiency of TPA autocorrelation in CdS bulk can be exceeded by about two orders, based of the enhancement of the two photon absorption coefficient in CdSe nanoplatelets relative to bulk (β_r = 8.8 cm GW^{-1} (ref. 2)). In addition, oriented CdSe NPLs show directional PL emission in the *z*-direction.[50] Hence, *e.g.* oriented multilayers can allow for high collection efficiency, for instance ideally matching a 0.4 NA detection optics.

It can be seen from the discussion above that autocorrelation with 2D semiconductors has higher efficiency, once very short interaction length is considered. Therefore TPA based autocorrelators have a great application potential for the characterization of ultrashort pulses. As the two-photon absorption spectrum is broad,[5] *i.e.* very high bandwidth (>100 nm), few fs pulses may be autocorrelated efficiently opening up great application perspectives. The performance of TPA autocorrelation with nanoplatelets in terms of efficiency for wavelength different than 800 nm or for large spectral bandwidth follows from the spectral course of TPA cross sections for CdSe nanoplatelets, measured in ref. 5.

Reasoned in the ultra strong electronic confinement, the very high TPA cross sections result in superiority of nanoplatelets over bulk semiconductor materials for autocorrelation, used in the past. Many of the discussed semiconductors were limited to a wavelength regime above 1 micron and were also quickly reaching intensity saturation limits for intense beams.[40] All these obstacles are not present with nanoplatelets, yielding high sensitivity and no saturation effects. Instead of detecting the luminescence externally, our NPLs can poss-

ibly be used in on-chip photonics, combining the large nonlinearities and resulting high sensitivities with direct detection of the two photon induced luminescence. For example nanoplatelets can be deposited on a planar photodiode, which detects the autocorrelation related PL with high efficiency. Especially due to the fact, that this PL emission is directional,[50] and mainly in the direction of the surface normal of nanoplatelets such a structure will provide high efficiency. Advances towards the processing and characterization of quantum confined CdSe particles in optoelectronics have already been made.[51,52] We also remark that conventional (epitaxial) II–VI quantum wells will not be able to compete with these structures, as due to *e.g.* interface roughness scattering the exciton coherence areas (volumina) do not reach the platelet values, resulting presumably in considerably lower nonlinearities and hence autocorrelation efficiencies. Further, as in such epitaxial structures the dielectric mismatch between the CdSe quantum well and surrounding (*e.g.* $Zn_xCd_{1-x}Se$) material is low, the excitonic correlation is considerably lower and therefore the exciton Bohr radius is higher. This results in lower transition dipole moments,[21] concatenated for the two photon transition, and due to second order Fermi's Golden Rule in considerably smaller TPA rates. We remark that the efficiency of autocorrelation can be further enhanced considerably by using larger nanoplatelets as the ones used in this study. Their TPA cross sections can be with $\sim 10^8$ GM (ref. 5) even a hundred times higher, further enhancing the autocorrelation efficiency. Hence II–VI nanoplatelets are a favored system for TPA based autocorrelation.

3. Conclusion

We have shown that CdSe nanoplatelets can be used for a new class of semiconductor broadband autocorrelators with unprecedented sensitivity. Collecting two-photon induced fluorescence, we measured pulse durations of fs laser pulses using different CdSe NPLs and a CdS bulk sample. We obtained very good agreement of the TPA based methods with conventional BBO based SHG pulse width measurements. In addition, we have demonstrated very high two-photon absorption cross sections and saturation intensities, which are related to strong anisotropic confinement and in-plane wave function coherence in CdSe nanoplatelets. They lead to very high autocorrelation efficiencies, which can be two orders of magnitude higher as conventional techniques, especially for short interaction length. Apart from the exceptional sensitivity, a main advantage, however, is the large potential cross- and auto correlation bandwidth allowing autocorrelation of (<10) fs pulses. The total efficiency could be further boosted if *e.g.* larger nanoplatelets are used or the nanoplatelets are deposited directly atop a planar photodiode, so that all PL is detected *via* the photodiode. This diode should have higher bandgap than the fundamental laser pulses, but lower than the emitted PL. In such a scheme the high nonlinearity of nanoplatelets could be combined with even higher detection efficiency. Also the nanoplatelets can by synthesiszed from many II–VI material combinations, so that a broad range of spectral regions for autocorrelation can be accessed.

4. Methods

CdSe nanoplatelets[50] of 4.5 ML thickness and 24×12 nm^2 and 29×6 nm^2 lateral size were dispersed in a polystyrene (PS) matrix as follows: In a vessel, 1 g of PS beads were mixed with 4 mL of toluene and heated to 60 °C while stirring. After 2 h, the solution was left to cool to room temperature. Subsequently, CdSe NPLs dispersed in hexane were mixed with the PS solution and left to dry at room temperature to produce the CdSe NPL-doped PS film. Details of the CdSe NPL synthesis are described in ref. 53. Size and shape of the NPLs were determined by TEM. See also ESI† for further details. A hexagonal CdS wafer (0.5 mm thickness) with *c*-axis perpendicular to the surface ((0001) orientation) is used as a two photon autocorrelation reference. For our autocorrelation measurements the beam of a 171 fs Titan-Sapphire-Laser (Coherent Mira-HP) operated at 800 nm was split into two parts and both focused onto the sample in a symmetric, but non-collinear geometry with a relative angle of ~10°. The geometry is shown in Fig. 1. In case of SHG autocorrelation *via* a 0.5 mm BBO crystal, the phase matching angle was found *via* optimizing the generated SHG, coupled *via* a lens to a spectrometer. To autocorrelate the pulses in case of the CdS and CdSe samples, the fluorescence was collected by a 0.25 NA objective and focused on the entrance slit of a BW&TEk BRC111A spectrometer.

Conflicts of interest

There are no conflicts of interest to declare.

Acknowledgements

A. W. A. acknowledges funding by DFG project number AC290-2/1. Additionally, this project has received funding from the European Research Council (ERC) under the European Union's Horizon 2020 research and innovation program (I. M., grant agreement no. 714876 PHOCONA).

References

1 S. A. Blanton, M. A. Hines, M. E. Schmidt and P. Guyot-Sionnest, *J. Lumin.*, 1996, **70**, 253–268.
2 J. He, J. Mi, H. Li and W. Ji, *J. Phys. Chem. B*, 2005, **109**, 19184–19187.
3 X. Feng and W. Ji, *Opt. Express*, 2009, **17**, 13140.
4 X. Li, J. van Embden, J. W. M. Chon and M. Gu, *Appl. Phys. Lett.*, 2009, **94**, 103117.

5 R. Scott, A. W. Achtstein, A. Prudnikau, A. Antanovich, S. Christodoulou, I. Moreels, M. Artemyev and U. Woggon, *Nano Lett.*, 2015, **15**, 4985–4992.
6 M. Allione, A. Ballester, H. Li, A. Comin, L. Movilla, J. I. Climente, I. Moreels and L. Manna, *ACS Nano*, 2013, **7**, 2443–2452.
7 A. W. Achtstein, A. Ballester, J. L. Movilla, J. Hennig, J. I. Climente, A. Prudnikau, A. Antanovich, R. Scott, M. V. Artemyev, J. Planelles and U. Woggon, *J. Phys. Chem. C*, 2015, **119**, 1260–1267.
8 G. L. Dakovski and J. Shan, *J. Appl. Phys.*, 2013, **114**, 014301.
9 A. W. Achtstein, J. Hennig, A. Prudnikau, M. V. Artemyev and U. Woggon, *J. Phys. Chem. C*, 2013, **117**, 25756–25760.
10 M. Nyk, J. Szeremeta, D. Wawrzynczyk and M. Samoc, *J. Phys. Chem. C*, 2014, **118**, 17914–17921.
11 J. Heckmann, R. Scott, A. V. Prudnikau, A. Antanovich, N. Owschimikow, M. Artemyev, J. I. Climente, U. Woggon, N. B. Grosse and A. W. Achtstein, *Nano Lett.*, 2017, **17**, 6321–6329.
12 E.-S. Wu, J. H. Strickler, W. R. Harrell and W. W. Webb, *Optical/Laser Microlithography V*, 1992.
13 B. Guzelturk, Y. Kelestemur, M. Olutas, S. Delikanli and H. V. Demir, *ACS Nano*, 2014, **8**, 6599–6605.
14 C. She, I. Fedin, D. S. Dolzhnikov, A. Demortière, R. D. Schaller, M. Pelton and D. V. Talapin, *Nano Lett.*, 2014, **14**, 2772–2777.
15 M. Li, M. Zhi, H. Zhu, W.-Y. Wu, Q.-H. Xu, M. H. Jhon and Y. Chan, *Nat. Commun.*, 2015, 8513.
16 R. Schropp, J. de Wild, W. van Sark, A. Meijerink, J. Feenstra and J. Schermer, Materials Challenges in Alternative & Renewable Energy (MCARE 2016); Symposium 2: Spectral Conversion Materials for Energy Applications; S2-001 April 18, 2016, 2016.
17 E. Petryayeva, W. Russ Algar and I. L. Medintz, *Appl. Spectrosc.*, 2013, **67**, 215–252.
18 F. Wang, D. Banerjee, Y. Liu, X. Chen and X. Liu, *Analyst*, 2010, **135**, 1839–1854.
19 V. Biju, T. Itoh, A. Abdulaziz, A. Sujith and M. Ishikawa, *Anal. Bioanal. Chem.*, 2008, **391**, 2469–2495.
20 K.-L. Chou, N. Won, J. Kwag, S. Kim and J.-Y. Chen, *J. Mater. Chem. B*, 2013, **1**, 4584.
21 J. Planelles, A. W. Achtstein, R. Scott, N. Owschimikow, U. Woggon and J. I. Climente, *ACS Photonics*, 2018, **5**, 3680–3688.
22 A. W. Achtstein, R. Scott, S. Kickhöfel, S. T. Jagsch, S. Christodoulou, G. H. Bertrand, A. V. Prudnikau, A. Antanovich, M. Artemyev, I. Moreels, A. Schliwa and U. Woggon, *Phys. Rev. Lett.*, 2016, **116**, 116802.
23 A. W. Achtstein, A. Schliwa, A. Prudnikau, M. Hardzei, M. Artemyev, C. Thomsen and U. Woggon, *Nano Lett.*, 2012, **12**, 3151–3157.
24 S. Ithurria and B. Dubertret, *J. Am. Chem. Soc.*, 2008, **130**, 16504–16505.
25 A. Antanovich, A. W. Achtstein, A. Matsukovich, A. Prudnikau, P. Bhaskar, V. Gurin, M. Molinari and M. Artemyev, *Nanoscale*, 2017, **9**, 18042–18053.
26 A. W. Achtstein, O. Marquardt, R. Scott, M. Ibrahim, T. Riedl, A. V. Prudnikau, A. Antanovich, N. Owschimikow, J. K. N. Lindner, M. Artemyev and U. Woggon, *ACS Nano*, 2018, **12**, 9476–9483.
27 J. Q. Grim, S. Christodoulou, F. Di Stasio, R. Krahne, R. Cingolani, L. Manna and I. Moreels, *Nat. Nanotechnol.*, 2014, **9**, 891–895.
28 R. Scott, A. V. Prudnikau, A. Antanovich, S. Christodoulou, T. Riedl, G. H. V. Bertrand, N. Owschimikow, J. K. N. Lindner, Z. Hens, I. Moreels, M. Artemyev, U. Woggon and A. W. Achtstein, *Nanoscale*, 2019, **11**, 3958–3967.
29 J. F. Specht, R. Scott, M. Corona Castro, S. Christodoulou, G. H. V. Bertrand, A. V. Prudnikau, A. Antanovich, L. D. A. Siebbeles, N. Owschimikow, I. Moreels, M. Artemyev, U. Woggon, A. W. Achtstein and M. Richter, *Nanoscale*, 2019, **11**, 12230–12241.
30 Y. Takagi, T. Kobayashi, K. Yoshihara and S. Imamura, *Opt. Lett.*, 1992, **17**, 658–660.
31 H. K. Tsang, L. Y. Chan, J. B. D. Soole, H. P. LeBlanc, M. A. Koza and R. Bhat, *Electron. Lett.*, 1995, **31**, 1773–1775.
32 Y. Takagi, *Appl. Opt.*, 1994, **33**, 6328–6332.
33 F. R. Laughton, J. Marsh, D. Barrow and E. Portnoi, *IEEE J. Quantum Electron.*, 1994, **30**, 838–845.
34 L. Barry, P. Bollond, J. Dudley, J. Harvey and R. Leonhardt, *Electron. Lett.*, 1996, **32**, 1922–1923.
35 J. K. Ranka, A. L. Gaeta, A. Baltuska, M. S. Pshenichnikov and D. A. Wiersma, *Opt. Lett.*, 1997, **22**, 1344–1346.
36 W. Rudolph, M. Sheik-Bahae, A. Bernstein and L. F. Lester, *Opt. Lett.*, 1997, **22**, 313–315.
37 Z. Zheng, A. M. Weiner, J. H. Marsh and M. M. Karkhanehchi, *IEEE Photonics Technol. Lett.*, 1997, **9**, 493–495.
38 N. F. Kleimeier, T. Haarlammert, H. Witte, U. Schühle, J.-F. Hochedez, A. BenMoussa and H. Zacharias, *Opt. Express*, 2010, **18**, 6945–6956.
39 D. T. Reid, M. Padgett, C. McGowan, W. E. Sleat and W. Sibbett, *Opt. Lett.*, 1997, **22**, 233–235.
40 D. Reid, W. Sibbett, J. Dudley, L. Barry, B. Thomsen and J. Harvey, *Appl. Opt.*, 1998, **37**, 8142–8144.
41 B. V. Emmanuel Rosencher, *Optoelectronics*, Cambridge Univ. Press, 2002.
42 M. Hassan, A. Wirth, I. Grguras, T. T. Luu, A. Moulet, V. Yakovlev, J. Gagnon, O. Razskazovskaya, R. Santra, S. Pabst, A. Azzeer, Z. Alahmed, V. Pervak, F. Krausz and E. Goulielmakis, *Attosecond physics with Synthesized Transients of Light*, 2012, p. LW4H.2.
43 J.-C. Diels and W. Rudolph, *Ultrashort Laser Pulse Phenomena*, Academic Press, Burlington, 2nd edn, 2006, pp. 457–489.
44 G. Agrawal, *Nonlinear Fiber Optics*, Academic Press, Boston, 5th edn, 2013, pp. 57–85.
45 N. Sultanova, S. Kasarova and I. Nikolov, *Acta Phys. Pol., A*, 2009, **116**, 585–587.
46 J.-C. Diels and W. Rudolph, *Ultrashort Laser Pulse Phenomena (Second Edition)*, Academic Press, Burlington, 2nd edn, 2006, pp. 1–60.

47 G. He, *Nonlinear Optics and Photonics*, Oxford Univ. Press, 2014.
48 Z. Hens and I. Moreels, *J. Mater. Chem.*, 2012, **22**, 10406–10415.
49 R. W. Boyd, *Nonlinear Optics*, Academic Press, Burlington, 3rd edn, 2008.
50 R. Scott, J. Heckmann, A. V. Prudnikau, A. Antanovich, A. Mikhailov, N. Owschimikow, M. Artemyev, J. I. Climente, U. Woggon, N. B. Grosse and A. W. Achtstein, *Nat. Nanotechnol.*, 2017, 1155–1160.
51 X. Geng, L. Niu, Z. Xing, R. Song, G. Liu, M. Sun, G. Cheng, H. Zhong, Z. Liu, Z. Zhang, L. Sun, H. Xu, L. Lu and L. Liu, *Adv. Mater.*, 2010, **22**, 638–642.
52 A. Robin, E. Lhuillier, X. Z. Xu, S. Ithurria, H. Aubin, A. Ouerghi and B. Dubertret, *Sci. Rep.*, 2016, **6**, 24909.
53 G. H. V. Bertrand, A. Polovitsyn, S. Christodoulou, A. H. Khan and I. Moreels, *Chem. Commun.*, 2016, **52**, 11975–11978.